Available online at www.sciencedirect.com
SCIENCE DIRECT
Earth and Planetary Science Letters 241 (2006) 672–685
EPSL
www.elsevier.com/locate/epsl

Raman micro-spectroscopy on diamond, graphite and other carbon polymorphs from the ultrahigh-pressure metamorphic Kimi Complex of the Rhodope Metamorphic Province, NE Greece

Maria Perraki [a,b,*], Alexander Proyer [b], Evripidis Mposkos [a], Reinhard Kaindl [b,c], Georg Hoinkes [b]

[a] School of Mining and Metallurgical Engineering, National Technical University of Athens, 9 Heroon Politechniou St., Zografou, Athens, GR-15780, Greece
[b] Institute of Earth Sciences, University of Graz, Universitaetsplatz 2, A-8010, Austria
[c] Institute of Mineralogy and Petrography, University of Innsbruck, Innrain 52, A-6020, Austria

Received 25 January 2005; received in revised form 3 October 2005; accepted 8 November 2005
Available online 20 December 2005
Editor: V. Courtillot

Abstract

Raman micro-spectroscopy was applied on carbon inclusions in garnet porphyroblasts from kyanite–biotite–garnet schists of the Rhodope Metamorphic Province (RMP), NE Greece. Diamond and cuboids of poorly to highly ordered graphite were identified either as single phase inclusions or as polyphase inclusions along with CO_2 and/or carbonates (calcite/magnesian calcite). Questionable Raman bands that may be assigned to other C-phases (?nanodiamond/?lonsdaleite/?a different C-polymorph) have been observed. The presence of diamond confirms beyond any doubt the ultrahigh-pressure (UHP) metamorphism reported by Mposkos and Kostopoulos [1] [E. Mposkos, D. Kostopoulos, Diamond, former coesite and supersilisic garnet in metasedimentary rocks from the Greek Rhodope: a new ultrahigh-pressure metamorphic province established, Earth Planet. Sci. Lett. 192 (2001) 497–506] in the RMP. Cuboid graphite showing variable degree of disordering most probably formed after diamond. The possible involvement of CO_2 and or C–O–H fluids in the formation of diamond is discussed.

Keywords: Rhodope Metamorphic Province; Kimi Complex; ultrahigh-pressure metamorphism; Raman micro-spectroscopy; diamond; disordered graphite

1. Introduction

Raman micro-spectroscopy is a proven and very important non-destructive characterization tool for distinguishing micro-sized particles of C-polymorphs, as it is very sensitive to the nature of carbon bonding. A typical application is the in situ identification of inclusions of C-polymorphs (diamond–graphite) in thin sections of metamorphic rocks, providing unambiguous evidence of UHP metamorphism (e.g., [2–5]). The UHP metamorphism of the RMP first reported by Mposkos and Kostopoulos [1], followed by Mposkos et al. [6], Mposkos [7] and Liati et al. [8], has proven controversial. Beyssac and Chopin [9] argued that the Raman spectrum of a C-polymorph ascribed to dia-

* Corresponding author. School of Mining and Metallurgical Engineering, Division of Geo-Sciences, National Technical University of Athens, 9 Heroon Politechniou St., GR-15773, Zografou (Athens), Greece. Tel.: +30 210 7722115; fax: +30 210 7722126.
E-mail address: maria@metal.ntua.gr (M. Perraki).

0012-821X/$ - see front matter © 2005 Elsevier B.V. All rights reserved.
doi:10.1016/j.epsl.2005.11.014

mond nanodomains by Mposkos and Kostopoulos [1] was rather that of disordered graphite. Besides, oriented rods of quartz and apatite and needles of rutile in sodic garnet from kyanite–biotite gneiss [1] and clinopyroxene blebs in garnet with oriented rutile from a metabasite [8] proposed as UHP mineral indicators were highly disputed as not being indicative of UHP [9,10].

Challenged by this controversial discussion on the possible presence of diamond in the RMP we carried out a thorough micro-Raman study of carbon microinclusions in garnets from metapelites from the RMP. In the present paper, we document the UHP metamorphism by the unequivocal presence of diamond and discuss the aspects involved in interpreting the spectra as well as the possible nature of diamond formation.

2. Geological setting

The Rhodope Metamorphic Province (RMP) in Northern Greece has been traditionally viewed as a stable continental block, consolidated in Precambrian to Palaeozoic times (e.g., [11,12]). However, thorough structural, petrological and radiometric studies over the last 20 yr have shown the RMP in fact to be a complex of Alpine synmetamorphic nappes characterized by south to southwestward stacking and associated with both coeval and subsequent extension in an Alpine active margin setting [13–26].

Mposkos and Krohe [25] and Krohe and Mposkos [26] have further subdivided the RMP into discrete entities on the basis of calculated metamorphic *P–T* paths and exhumation age criteria for the various metamorphic rocks (Fig. 1). Thus, the earliest exhumed and structurally uppermost entity is the Kimi Complex (65–48 Ma), followed by the Sidironeron (Central Rhodope) and Kechros (East Rhodope) Complexes (42–30 Ma) and then by the Pangaeon Complex (26–8 Ma) which also forms the well-defined Rhodope metamorphic core complex.

The Kimi Complex consists of continental crustal and mantle rocks. Predominant are migmatitic quartz–feldspar gneisses, kyanite-bearing pelitic schists and paragneisses, marbles, amphibolites and basic granulites that locally preserve eclogitic textures and compositions, dioritic to granitic metaplutons as well as an ultramafic association mostly made up of metaperidotites and subordinate garnet pyroxenites [27]. Widespread pegmatites intersect the lithological succession.

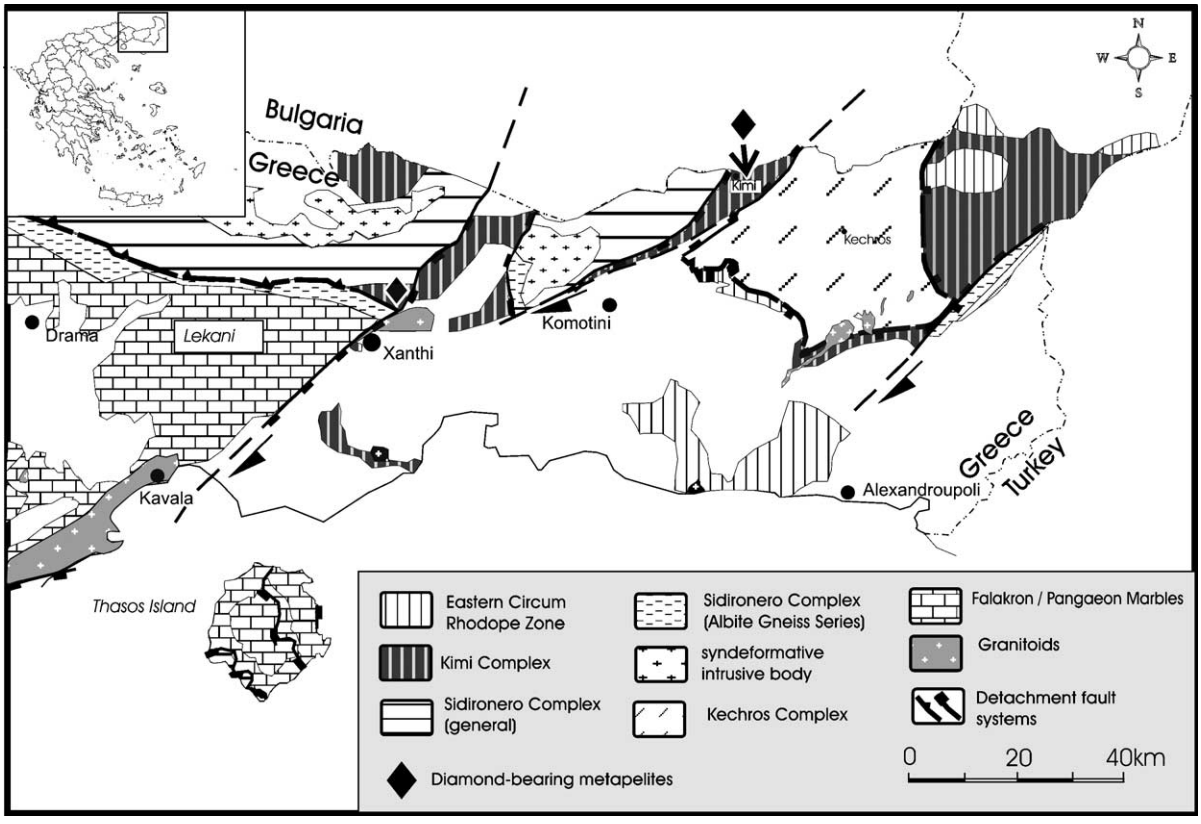

Fig. 1. Simplified geotectonic map of East Rhodope after Krohe and Mposkos [26]. Xanthi and Kimi areas are marked on the map.

Tiny cuboids of diamond and graphite were discovered as μm-sized inclusions in garnet from metapelitic schists of the Kimi Complex near Kimi village and north of Xanthi town (Fig. 1).

3. Petrography–mineral chemistry

The pelitic schists and gneisses of the Kimi Complex are very uniform in their mineralogy. The paragenesis consists of coarse-grained garnet+kyanite+muscovite+biotite+quartz+plagioclase+rutile; staurolite and chlorite are replacing kyanite, biotite and garnet at a late stage and ilmenite is replacing rutile. Garnet porphyroblasts show resorbed rims and are commonly replaced by biotite, kyanite and plagioclase. Kyanite shows two distinct fractions of grain size; large kyanite porphyroblasts (ky1) up to 1 cm in length associated with garnet porphyroblasts and small kyanite grains (ky2) associated with biotite and replacing garnet. The formation of ky2 reflects a late stage of major recrystallization in the upper amphibolite facies with garnet+phengite reacting to kyanite+biotite+quartz. Muscovite coexists with biotite of equal grain size and is more rarely replaced by small biotite flakes along grain boundaries. The primary paragenesis, which is shown in the following to have formed within the diamond stability field, was presumably garnet+phengite+clinopyroxene+coesite+rutile. The mineral chemistry, petrology and *PT*-evolution of these rocks will be described elsewhere. At this point we only briefly describe garnet, the host of the carbon inclusions.

Garnets are generally homogeneous in composition. Only a retrograde zoning is developed in the outermost rim with decreasing Mg and increasing Fe, Mn and Ca depending on the neighbouring mineral [18]. Even though the extraordinary composition of garnet at UHP-conditions, with significant amounts of Ti, P and Na [1], is very rarely preserved and garnet is often strongly resorbed by biotite, kyanite and plagioclase, extremely fine grained rutile needles can be found in garnets of almost any of the Kimi metapelite samples. These rutile needles are strictly aligned in up to three observable crystallographic directions of the garnet host and evenly or patchily distributed throughout the garnet, with strong variations in abundance. Microprobe and Raman analyses revealed the presence of other rarer oriented phases, mainly quartz and apatite (usually less than 10 rods per garnet grain for quartz and even less for apatite) that occur along with the rutile needles.

Fluid and solid micro-inclusions in garnet are very common [28,29]. The dominant fluid phase is CO_2, but minor amounts of N_2 and low-salinity H_2O-inclusions were also found. Solid micro-inclusions of C-polymorphs (diamond, graphitized diamond, ordered/disordered graphite), carbonates (calcite, magnesian calcite), quartz and kyanite are abundant in most of the garnets. The distribution of the fluid and solid micro- inclusions (especially CO_2, C-polymorphs and carbonates) in garnets is irregular and differs from garnet to garnet. In some cases, they are concentrated in the core of the garnet, in some others near the garnet rim while swarm-like trails of such inclusions are also observed. There is no apparent relationship to the oriented rutile needles and quartz and apatite rods.

4. Analytical methods

Raman spectra were obtained with a Jobin-Yvon TM LabRam-HR 800 Raman micro-spectrometer at the Institute of Earth Sciences of the University of Graz, Austria. Spectra were excited at room temperature with the 633 nm line of a 5.9 mW He–Ne laser through an OLYMPUSTM 100X objective. Numerical aperture of the objective is 0.9. Focal length of spectrometer is 800 mm. The laser spot on the surface had a diameter of approximately 1 μm and a power of 1 mW, which should be low enough to avoid any spectral change or sample destruction due to light absorption and local temperature increase [30]. The entrance slit into the spectrometer was set to 20 μm. Light was dispersed by a holographic grating with 1800 grooves/mm. The spectral resolution of about 0.6 cm^{-1} was determined by measuring the Rayleigh line of the He–Ne laser. The dispersed light was collected by a 2048×512 back illuminated low noise UV CCD detector. A confocal pinhole was not used; confocality was achieved by setting the entrance slit into the spectrometer to 20 μm and selecting via software few relevant rows on the CCD, a so-called "virtual" pinhole. The depth resolution of this "pseudo-confocal" configuration is usually better than 2 μm (application note no. 01, Jobin-Yvon, 2000). All spectra were recorded at parallel orientation of the incident laser beam and the scattered light. The "scanning" mode was selected in order to avoid step-like mismatches between neighboring spectral windows probably occurring in samples with intense and uneven background and to maximize the signal-to-noise ratio [4,31]. All spectra were baseline corrected by subtraction of line segments and fitted to Gauss–Lorentz. Deviations between measured FWHM and for the so-called apparatus function mathematical corrected FWHM [32–34] were lower than 0.2 cm^{-1} and hence not corrected. Wavenumber calibration was done by regular measuring the position of the Rayleigh

line. Wave number accuracy achieved by this method is around 0.5 cm^{-1}.

5. Raman micro-spectroscopy on C-phases included in garnets from metapelites

5.1. General remarks

Diamonds are known to show Raman active triply degenerate first-order F2g phonon at 1332 ± 0.5 cm^{-1} with a typical full width at half maximum (FWHM) of 1.65 ± 0.02 cm^{-1} at room temperature [35]. Distortions from the perfect cubic lattice, such as variations in bond length and angle, influence both the width and position of this line. Shift of this band to higher/lower wave numbers indicates compressive/tensile stress in the lattice and an increased width of this band reflects an increase in structural disorder or very small crystal sizes [36]. Diamonds also show a second-order Raman spectral feature that extends from 2200 to 2800 cm^{-1} with a sharp band at 2600 cm^{-1} [37].

The Raman spectrum of carbonaceous material is highly sensitive to its crystallinity. It consists of 1st-order (1100–1800 cm^{-1}) and 2nd-order (2500–3100 cm^{-1}) regions [38,39]. In the 1st-order region a single Raman mode (G band) is expected in the 1300–1600 cm^{-1} region for well-ordered graphite with a band position near 1580 cm^{-1} [38–40] and it corresponds to in-plane vibration of aromatic carbons in the graphitic structure. An additional band near 1350 cm^{-1} (D_1) and a shoulder at 1620 cm^{-1} (D_2) are typically observed in disordered carbonaceous material [41–44]. These defect bands have been attributed to in-plane defects and heteroatoms [45]. The D_1 band of carbonaceous material has been shown to have a strong dispersive character (Raman band shift with excitation wavelength, [46–49]). In the 2nd-order region several bands have been mentioned to appear at 2400, 2700, 2900 and 3300 cm^{-1} ([39,44]) corresponding to overtone and combination scattering.

All the phases described below were identified as micro-inclusions in diamond-bearing garnet porphyroblasts from Kimi and Xanthi areas.

5.2. Diamonds

Diamonds with a size ranging from 3 to 9 μm were identified as inclusions in garnets from Kimi and Xanthi area. They occur either as isolated grains or as part of crystallographically controlled swarms. Most of them are single-phase inclusions; composite inclusions of diamond+carbonate (calcite/magnesian calcite) were also identified. As none of these carbonates has yet been found at the thin section surface, their actual composition is yet undetermined. The textural relation between diamond and carbonate cannot be documented with any certainty, at the optical microscopy scale, due to their very small size, unless high resolution SEM or TEM analyses will be performed.

The Raman active triply degenerate first-order F2g phonon of single diamonds appears as a sharp band between 1331 and 1332 cm^{-1} with full width at half maximum (FWHM) in the range of 2.2 to 4.6 cm^{-1}. In the biphased diamond+carbonate inclusions Raman bands of diamonds occur at ~1332 cm^{-1} with FWHM from 2.2 to 3.7 cm^{-1}. Taking into account the errors in wavenumber accuracy and the spectral resolution there is no general correlation between the Raman shift and the FWHM. The dominant band of the carbonate, assigned to symmetric stretching of planar CO_3 group [50] occurs at 1085 and 1087 cm^{-1}.

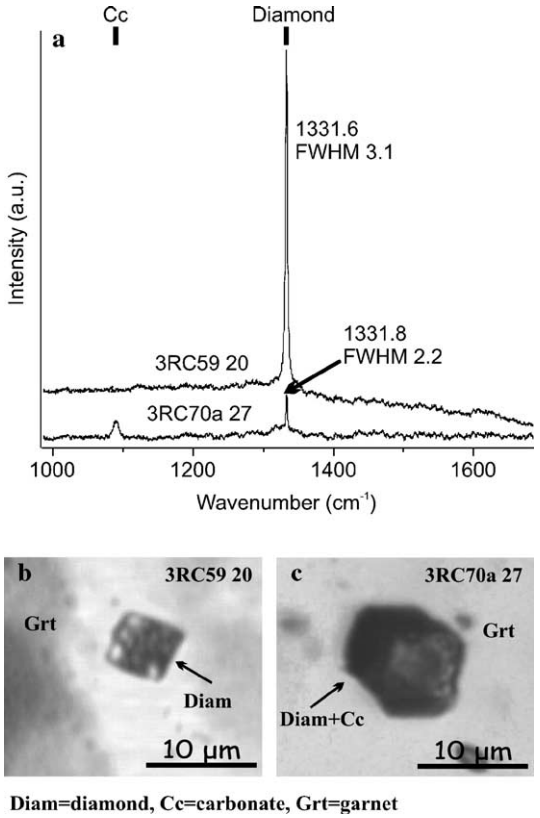

Fig. 2. (a) Typical Raman spectra of a single diamond inclusion (3RC59 20) in garnet from the Kimi area and a composite diamond+carbonate inclusion (3RC70a 27) in garnet from the Xanthi area. (b) Photomicrograph of the inclusion 3RC59 20. (c) Photomicrograph of the inclusion 3RC70a 27.

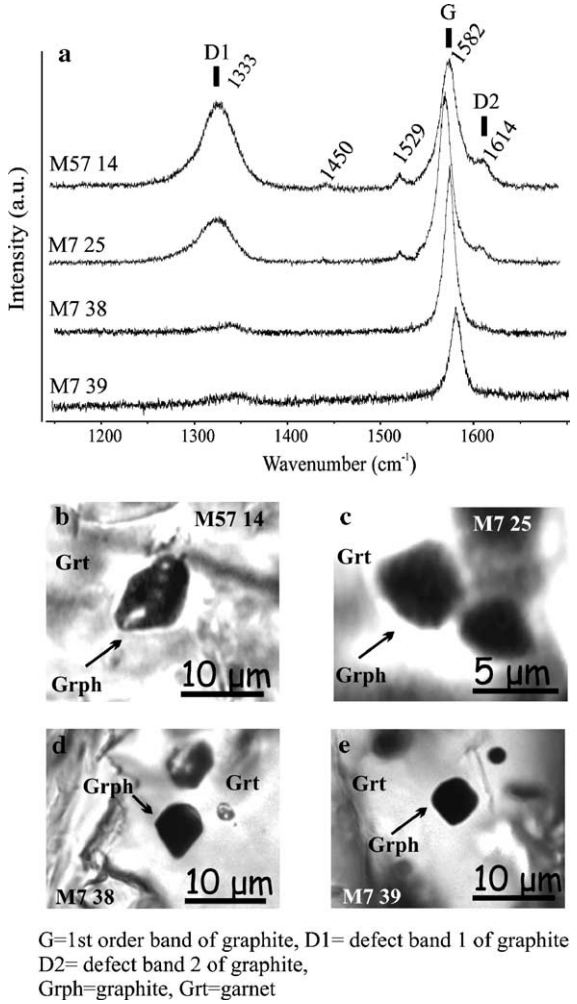

Fig. 3. (a) Raman spectra of graphitic carbon inclusions with varying degree of disordering. (b) Photomicrograph of the inclusion M57 14. (c) Photomicrograph of the inclusion M57 25. (d) Photomicrograph of the inclusion M7 38. (e) Photomicrograph of the inclusion M7 39.

Typical Raman spectra of a single microdiamond inclusion from Kimi area (Samples 3RC59) and a biphased diamond–carbonate inclusion from Xanthi area (Sample 3RC70a) are given in Fig. 2.

As it has been claimed that diamond can be an artifact of thin-section preparation (as residual particles from the diamond saw or the polishing material), we carefully checked the position of the diamond grains with respect to the polishing surface. With the exception of two cases in which the diamonds penetrate to the surface, all other diamonds are *completely enclosed* by garnet. Moreover, in the case of Sample 3RC70 in which 6 diamonds were identified, a second polished thin section was prepared without using diamond-bearing abrasives during thin section preparation. Diamond micro-inclusions in garnet porphyroblasts were also identified and verified by Raman micro-spectroscopy in this second thin section.

5.3. Highly ordered graphites

Cuboid carbon inclusions with typical Raman spectra of highly ordered graphite were also identified in diamond-bearing garnet porphyroblasts. Graphite shows a sharp first-order Raman band at 1581–1584 cm^{-1} with a FWHM of 13.5–13.7 cm^{-1}.

5.4. Disordered graphites

Cuboid inclusions of disordered graphitic carbon characterized by random distribution occur throughout the garnet grains. They occur either as single phases or as composite inclusions with CO_2 and/or carbonate.

First order Raman spectra were analyzed from 100 to 1800 cm^{-1}; in some cases the spectral range from 100 to 3400 was analyzed in order to check also for the second-order Raman bands. Representative Raman spectra of analyzed disordered graphites are presented in Fig. 3.

They have two bands in the first-order region, at ~1330 and ~1580 cm^{-1}, with a shoulder at ~1618 cm^{-1}, and a broad second-order band at ~2666 cm^{-1}. Interestingly, not all graphites show the same degree of disordering (Fig. 3). The R_1 $[(D_1/G)_H]$ and R_2 $[[D_1/(D_1+G+D_2)]_A]$ parameters characterizing graphite crystallinity [51] are highly variable. The FWHM of the G band varies from 12.8 to 32.3 cm^{-1} and its position from 1578 to 1582 cm^{-1}. No correlation between the

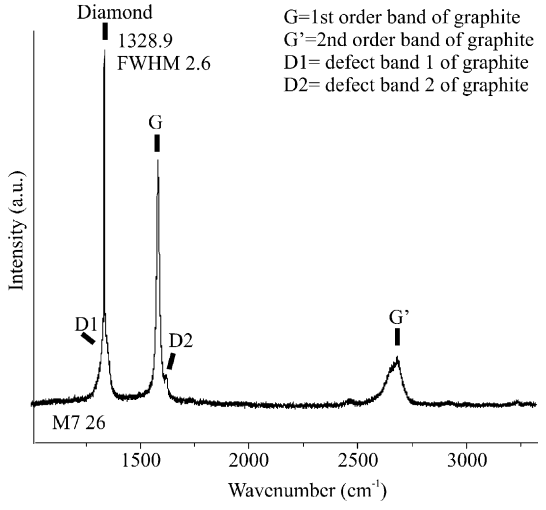

Fig. 4. Raman spectrum of a composite inclusion of diamond+disordered graphite in garnet.

degree of disordering and the areal distribution of graphite grains was observed.

In spectrum 57 14 (Fig. 3) two additional bands at 1449 and 1529 cm^{-1} are present. These two bands also appear weakly in spectrum M7 25.

5.5. Composite diamond–graphite inclusions

The Raman spectrum of a composite cuboid diamond–graphite inclusion (Sample M7, Kimi area) is given in Fig. 4. Both phases are easily recognized by the narrow band at 1329 cm^{-1} and the band at 1576 cm^{-1}, respectively. The FWHM of the diamond is 2.4 cm^{-1}. A slight broadening observed at the base of the diamond band could stem from the presence of a weak D_1 band in graphite, overlapped by the F2g mode of diamond. This assumption is strengthened by the presence of a shoulder on the graphite G band at 1619 cm^{-1} which is interpreted as the D_2 band that is always associated with the main D_1 band of disordered graphite.

Similar to the case of composite diamond+carbonate (§5.2) and (?) nano-diamond+CO_2+carbonate (§5.6) inclusions, it was unfeasible to determine the textural relation between diamond and graphite on an optical basis.

5.6. Possible nanodiamonds or lonsdaleite

Numerous composite inclusions of CO_2, carbonates and possibly diamond nanoparticles were found within the garnets. They are aligned and show parallel faces suggesting a crystallographic control by the host garnet. Typical Raman spectra of these composite inclusions are given in Fig. 5. There is a peculiar wedge-shaped band around 1330 cm^{-1} along with peaks of CO_2, carbonate and garnet. Remarkable features are: a) the significant broadening of this band b) the absence of a band at ~1580 cm^{-1} (G band of graphite) c) the presence of CO_2 and carbonate. Additionally, there are monomineralic (based on their Raman spectra) inclusions in garnets, also part of the crystallographically controlled swarms, characterized by broad Raman bands at ~1330 cm^{-1}.

Deconvolution of the broad Raman bands of both composite and monomineralic inclusions reveals that most of these bands are actually triplets that consist of two sharp bands at ~1307 and 1333 cm^{-1} (FWHM 17 and 23 cm^{-1}, respectively), and a very broad one at ~1348 cm^{-1} (FWHM 54 cm^{-1}; Fig. 5b).

Possible interpretations for the wedge-shaped bands, e.g., as representing diamond nanoparticles or lonsdaleite ("hexagonal diamond") are discussed below.

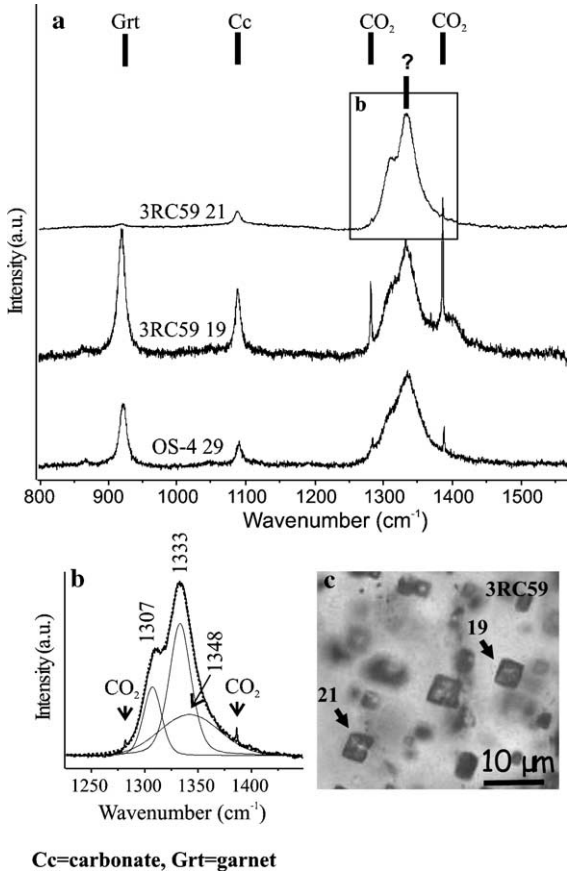

Fig. 5. (a) Raman spectra of representative composite inclusions of CO_2, calcite and (?) diamond nanoparticles. (b) Deconvolution of spectrum 3RC59 21 in the spectral range of 1225–1450 cm^{-1}. Heavy line indicates original spectrum, light lines deconvoluted Raman bands, stippled line band sum. See text for discussion. (c) Photomicrograph of the inclusions 3RC59 19 and 3RC59 21.

5.7. Other C-bearing micro-inclusions in garnet

Garnets of kyanite–biotite–garnet metapelites containing the above-described C-polymorphs are also rich in single micro-inclusions of carbonates and CO_2-rich fluids. They appear as negative crystals, that is, their shape and orientation are imposed by the garnet symmetry. In most of the cases they form intragranular crystallographically controlled swarms, along with diamond, graphite and multi-phased inclusions. Isolated and clustered micro-inclusions of carbonates and CO_2 fluids are also present.

5.7.1. Carbonates

Abundant, apparently single phase inclusions of carbonates, 3–20 μm in size, with straight grain boundaries, have been found in garnets of different samples of kyanite–biotite–garnet metapelites. Their Raman spec-

tra are very similar to the carbonate bands from the composite inclusions with ?nanodiamond/lonsdaleite+CO_2: a dominant band at 1085–1090 and secondary bands at 261–264, 289–297 and 707–710 cm^{-1}, which indicate compositions from calcite to magnesian calcite.

The Raman spectra of the carbonates at ambient conditions are well-known. The optical vibrations are internal vibrations of the CO_3 group (three Raman bands lying between 700 and 1500 cm^{-1}) and external or lattice vibrations involving translation and librations of the CO_3 groups relative to the Ca or Mg atoms (100–500 cm^{-1}). Calcite is characterized by a dominant Raman band at 1084 cm^{-1} and minor bands at 155, 281, 711, 1434 cm^{-1} and magnesite shows a dominant band at 1094 cm^{-1} and minor bands at 212, 329, 738, 1444 cm^{-1} [50,52,53]. Magnesian calcite inclusions in garnet porphyroblasts from the Dabie–Sulu terrane, China, have been reported to have Raman bands at 1087, 281 and 155 cm^{-1} (Fu, unpublished data, pers. comm.).

5.7.2. CO_2

The Raman spectrum of CO_2 generally consists of two bands, referred to as Fermi diad, at 1285 cm^{-1} (at 1 atm), and at 1388 cm^{-1}, usually called v_1 and $2v_2$, respectively [54,55].

CO_2 was found in single phase fluid inclusions, but also in composite inclusions of calcite+CO_2, C-polymorph+calcite+CO_2, graphite+CO_2. Both bands of CO_2 are characterized by a shift to lower wavenumbers; the v_1 band appears at ~1280–1282 cm^{-1} and the $2v_2$ band appears at ~1385–1386 cm^{-1}. The shift of the v_1 band is greater than the shift of the $2v_2$ band. These shifts can be explained by the influence of pressure (internal fluid pressure). Downshifts of 5 and 3 cm^{-1} of the v_1 and $2v_2$ band positions, respectively, with pressure increase have been mentioned by Garrabos et al. [54]. Extreme pressure conditions have been reported to be present in superdense CO_2 inclusions [53,55,56].

A detailed microthermometric and micro-Raman study on the fluid inclusions in the diamond-bearing metapelitic garnets will be presented elsewhere (Kaindl et al., in preparation).

6. Discussion

6.1. The nature of disordered graphite

Disordering in graphite is principally caused by in-plane defects and/or heteroatoms [45]. Four possible mechanisms of obtaining disordered graphite have been observed and reported in the literature. We discuss each of these possibilities in the light of our own evidence. Disordering can be the result of:

6.1.1. Polishing during thin section preparation

It has been shown that polishing can cause severe disorder effects in the structure of graphite which will reflect on the Raman spectrum [44 and references there in]. Polishing induces changes in the upper several hundred Ångstroms of the graphite lattice ("Beilby layer", [57]). The partial disorder by polishing may overprint the original degree of ordering in graphite. In order to avoid any mechanical disruption of the carbonaceous material, we focused the laser onto carbonaceous material beneath the surface of the transparent host mineral (garnet) as proposed by Pasteris [58], since this is left unaffected by surface polishing.

6.1.2. The progressive transformation of organic material originally present in sedimentary rocks to graphite

In this case, the graphite that forms during the first stages of graphitization (diagenesis to low-grade metamorphism) is composed of short and misoriented aromatic layers and thus it is highly disordered [43,44,51,59,60]. The degree of disorder reduces systematically with increasing temperature and has been used as a geothermometer.

Natural graphitization is mainly controlled by temperature with some additional influence by pressure, duration of the metamorphic event and shear. In the first stages of graphitization, the carbonaceous substance is characterized by a high degree of disordering, caused by the presence of heteroatoms in the lattice. Well-crystallized graphite is crystallographically defined by an interplanar d value of exactly 3.35 Å. Solid carbon phases with $d_{(002)}>3.35$ Å result from the presence of heteroatoms such as oxygen, hydrogen and nitrogen in the structure and are referred to as "disordered graphites". During diagenesis and low-grade metamorphism the heteroatoms are gradually released and the distance between the planes decreases to the ideal value of 3.35 Å [61]. Apart from the chemical modification of the starting material, the transformation of short and misoriented aromatic layers in poorly organized carbonaceous material up to perfectly stacked layers in the triperiodic structure of graphite is also achieved by microtextural and structural changes. Pasteris and Wopenka [43], Wopenka and Pasteris [44], Yui et al. [59] and Beyssac et al. [51,60] have provided quantitative parameters on the degree of organization in metamorphic carbonaceous material by means of Raman micro-spectroscopy mostly based on the intensity ratio of the G and D modes. However, as long as the orientation of the sp^2 carbon

layers with respect to the electric field vector of the laser beam is unknown, the intensity ratio of the *G* and *D* modes provides only rough estimate of the crystallinity of the carbonaceous samples and therefore the width and asymmetry of the *G* mode are additionally used as a measure of the order/disorder carbon [62,63].

As mentioned above, Raman micro-spectroscopy on disordered graphitic carbon micro-inclusions in garnets from metapelites revealed that the degree of disordering is highly variable. The Raman spectra obtained are comparable to the spectra of disordered graphite of the chlorite to staurolite zone of Wopenka and Pasteris [44] and the greenschist facies of Yui et al. [59]. In addition, using the temperature correlation formula of Beyssac et al. [51] to the R_2 parameter [$R_2=[D_1/(D_1+G+D_2)]_A$], temperatures from 450 to 580 °C are derived [T (°C)$=-445R_2+641$). Such temperatures of metamorphism are way below the peak metamorphic temperatures for the Kimi Complex [7].

It must be noted here that once graphite has attained a certain degree of ordering/crystallinity it does not retrogress during subsequent metamorphism [61]. It is not possible for graphite enclosed in an inclusion to structurally retrogress; only prograde changes in crystallinity are possible [64]. So the observed degree of crystallinity is the highest that graphite has obtained during the metamorphic evolution of the host rock. Given that the analyzed disordered graphites found as inclusions in garnet porphyroblasts from metapelites have experienced the same metamorphic history as the garnet host, such highly varying degree of disordering could not be easily explained as a temperature effect. Moreover, if the disordered graphite had formed entirely by the progressive and continuous graphitization of original organic material, only flake- or bleb-shape would be expected and not cuboids.

6.1.3. Diamond–graphite phase transformation

Experimental data on the diamond–graphite phase transition under different conditions [65–67], limited data on natural samples [68–70] and theoretical modeling of the diamond–graphite phase transition [71,72] suggest the existence of intermediate disordered phases between diamond and graphite.

Gogotsi et al. [65,66] have experimentally studied the pressure-induced phase transformation in diamond. They carried out diamond–diamond indentation experiments, at ambient temperature and pressures of several hundred GPa, by pressing a sharp diamond indenter against its surface. In the point of indentation diamond is transformed to graphite with extremely high degree of disordering. A continuous range of Raman spectra from graphite to diamond (graphite→disordered graphite→diamond) has been reported in shock experiments by Kenkmann et al. [67]. Furthermore, graphites coexisting with diamonds in gneisses from the Ries Crater, Germany, show high degree of disordering [68]. Besides, Raman spectra of graphite pseudomorphs after diamond from the Maksyutov Complex are characteristic of disordered graphites [69]. In addition, Willems et al. [70] demonstrated that highly disordered polycrystalline graphite forms after high-temperature annealing in inert atmosphere of polycrystalline natural diamond. The diamond–graphite phase transition has also been modelled theoretically. Intermediate disordered phases of graphite with Csp^2 and Csp^3 and diamond with Csp^2 and Csp^3 are proposed to form between normal graphite (Csp^2) and diamond (Csp^3) [71]. Studies on graphitization at diamond dislocation cores suggest the formation of sp^2 carbon pairs as a first step [72].

The cuboid morphology of the analyzed disordered graphites is the most persuasive indication for graphitized diamond and combined with the presence of diamond and cubic diamond–graphite composite inclusions in the same garnet porphyroblasts imply that the *D* band in disordered graphite most probably arises from the distortion of the diamond structure during transformation to graphite. In this case the transformation of diamond to graphite is continuous with the formation of disordered graphite as intermediate phase.

6.1.4. Graphite precipitation from a fluid inclusion

A detailed study revealed that natural fluid-deposited graphite exhibits high degree of order [61]. However, graphite precipitating from a fluid inclusion, especially on the walls of fluid inclusion has been reported to exhibit disorder [44,64]. A detailed Raman spectroscopic study on graphite crystals within fluid inclusions in granulites of Nilgiri hills, India, showed that they possess varying degree of crystallinity [73].

In our case, the possibility of graphite nucleation from a CO_2 fluid or C–O–H fluid is corroborated by the presence of composite inclusions of graphite + CO_2 or graphite + CO_2 + carbonate.

Whereas graphite formed by in situ metamorphism shows a distinct and systematic increase in crystallinity with increasing grade of metamorphism, such a correlation has not been referred to and also not expected for fluid-deposited graphite or disordered graphite formed during the diamond–graphite phase transformation.

The random distribution of graphite with variable degree of disordering throughout garnet grains rules out the theoretical possibility of prograde entrapment and preservation of increasingly ordered graphite during

garnet growth but is compatible with precipitation from a fluid inclusion.

The distinction between the last two mechanisms of disordered graphite formation, i.e., whether all disordered and even ordered graphite had been diamond once and was transformed later on (case C), or whether diamond, disordered graphite and ordered graphite all grew within former fluid inclusions by precipitating at different stages along a decompression *PT*-path (case D), is difficult. A primary precipitation of disordered and ordered graphite from a fluid has been observed both in experiments [61] and in nature [73] and can be followed by solid state phase transformation, thus mimicking the case C. Primary fluid inclusions from high and even ultrahigh pressures are virtually impossible to preserve during exhumation of the rock, so decrepitation and even annealing of the decrepitated fluid trails during the late amphibolite to granulite facies stage have to be assumed for our rocks. Considering this *P–T* history, we believe that a combination of the last two cases may have taken place i.e., selective decrepitation and annealing of primary fluid inclusions from which carbon and carbonate phases subsequently precipitated combined with a solid-state transformation.

6.2. Nanodiamond and lonsdaleite

As mentioned above, composite and monomineralic inclusions showing broad Raman bands at ~1330 cm^{-1} were recorded. After deconvolution, these bands were shown to consist of two sharp bands at ~1307 and 1333 cm^{-1} and a broader one at ~1348 cm^{-1}.

There is no straightforward assignment for this peculiar broad wedge-shaped band of some inclusion spectra at ~1333 cm^{-1} (Fig. 5). Although a band at this position is characteristic of diamond it has also been shown to represent the D_1 defect band of graphite when excited with an He–Ne laser with $\lambda = 632.817$ nm [9,48]. However, the first-order band of graphite at ~1580 cm^{-1}, which is still always present in highly disordered carbonaceous material where the defect bands become dominant (e.g., [44,60]), is totally absent.

On the other hand, typical diamonds show a FWHM of the first-order Raman band of 1.65 ± 0.02 cm^{-1} [35], a value much lower than the line width of the band at ~1333 cm^{-1} of the measured inclusions (23 cm^{-1}). A broadening of the first-order Raman band of diamond has been observed in several cases and attributed to nanoparticles [74–78]. Yoshikawa et al. [74] measured the Raman spectrum of cluster diamond with nanometer size (55 Å), which was made from graphite powder under high temperature and high pressure and reported a line width of 32 cm^{-1}. Chen et al. [75] studied the graphitization process of nanodiamond (~50 Å) occurring during annealing at different temperatures, in argon ambient, and reported a line width of ~30.7 cm^{-1} for the Raman band of nanodiamond. Prawer et al. [76] observed a broadening of 10 cm^{-1} studying nanometre sized diamond powder by Raman spectroscopy. Moroz et al. [77] attributed the broadening (~10 cm^{-1}) of the Raman bands of impact diamonds from the Popigay (Taimyr/north-central Siberia) and Karsk (the Polar Urals) craters to the existence of nanoparticles. Extremely broad single Raman bands (FWHM ~200–400cm^{-1}) at 1326–1370 cm^{-1} were assigned to metamorphic microdiamond inclusions consisting of nanocrystalline diamond aggregates in garnets from Maksyutov Massif [78]. In most of the cases, the broadening of the Raman band is accompanied by a shift to lower wave numbers, a case not observed in our spectra. However, this is not a rule and also depends on the orientation of the crystal [36].

Another possible interpretation is that proposed by Chiem et al. [79] who attributed Raman bands at ~1329 cm^{-1} with FWHM ~53 cm^{-1} to lonsdaleite. Similar broad, and slightly downshifted Raman bands, identical to that acquired on a lonsdaleite standard from the Zapadnaya impactite, Ukraine (D.C.Smith, pers. comm.) have been also described for inclusions in zircons from the Straumen UHP eclogite in Norway and in gneiss from the Kokchetav massif, Kazakhstan [80,81] suspected to be lonsdaleite or disordered diamond.

A band at ~1315 cm^{-1} has been also ascribed tentatively to the hexagonal diamond (lonsdaleite, [65,82,83]). However, detailed descriptions of this phase and definite Raman spectra are not yet available in the literature.

Hexagonal diamond (lonsdaleite) can be formed allegedly by deformation-induced twinning of the cubic diamond structure [65]. It is also believed to form when meteoritic graphite hits the earth. The great heat and stress of the impact transforms the graphite into diamond but retains graphite's hexagonal crystal lattice. It was first identified from the Canyon Diablo meteorite at Barringer Crater in Arizona [84].

The interpretation of unusually broadened bands at the diamond position as suggestive of nanodiamond aggregates, lonsdaleite or some other "disordered" diamond structure may be confirmed by future TEM analyses. In the hypothetical case that the above-mentioned broad bands represent diamond nanoparticles another question arising is if the presence of nanodiamonds indicates the same extreme pressure conditions as that of diamonds. Badziag et al. [85] demonstrated that from

the physical point of view nanometre-sized diamonds in which the surface bonds are terminated with hydrogen atoms may actually be more stable than graphite clusters of the same size, an expectation that has recently been confirmed experimentally [76].

6.3. Raman shift and FWHM of microdiamonds

The Raman shifts in the measured microdiamond inclusions in garnets between 1329 and 1332 cm^{-1} deviate from typical values for macroscopic diamonds and the FWHM of the measured inclusions are unusually broad (2.2–4.6 cm^{-1}). Deviations between typical Raman shift and FWHM of macroscopic diamonds and metamorphic microdiamonds from UHPM terranes have been previously reported. Metamorphic microdiamonds in dolomitic marbles from the Kokchetav Massif showed band positions from 1330 to 1335 cm^{-1} and relatively large FWHM of 5.9–8.0 cm^{-1} [86]. Similar to the inclusions we studied, no correlation between the FWHM and the position of the main diamond band was detected [86,87]. Metamorphic microdiamonds included in zircons from the North Qinling Zone (Central China) yielded shifted Raman bands between 1331 and 1334 cm^{-1}, suggesting the presence of impurities [5].

Broadening of the Raman band means shortening of the phonon lifetime or the phonon mean free path [88]. Several reasons may cause increased FWHM and/or downshift of the F2g phonon of diamond: Increase of laser power and decrease of particle size, internal stress variations caused by grain boundaries, nitrogen impurities and structural defects [36,88,89]. Increased laser power can be excluded since in our experiments it was below 1 mW at the focal point which should prevent any spectral change or sample destruction due to local temperature increase. The lack of a general correlation between Raman shift and FWHM of microdiamond bands investigated in this and previous studies [5,86,87] suggests that in most of the cases more than one of the above mentioned reasons contribute to the observed variations.

6.4. The growth of diamonds

The composite inclusions of microdiamond + carbonate and (?) nano-diamond + CO_2 + carbonate and single diamond and graphite inclusions in swarm-like trails also containing carbonates and CO_2-rich fluids in garnet porphyroblasts suggest the presence of H_2O–CO_2 fluid during UHP metamorphism in the diamond stability field and the close relationship between fluids and diamond formation.

Crystallisation of diamond from a supercritical CO_2 or C–O–H fluid has been studied experimentally (e.g., [90,91]) and proposed as a formation mechanism of natural metamorphic diamonds (e.g., [92–94]). It has been shown that supercritical CO_2 acts as a diamond-forming solvent catalyst [91]. Carbonates have been also reported to be such catalysts under high pressure–high temperature conditions (e.g., [95–99]). Intergrowths of carbonate with diamond have been described in garnet [100] and clinopyroxene (Korsakov and Hermann, unpublished data) from diamond-bearing dolomite marbles in Kokchetav UHP carbonate rocks.

Recently, the possibility of formation of carbonate melts in deeply subducted crustal rocks has been discussed. Magnesian calcite inclusions in garnet and occasionally in clinopyroxene, which display typical textures of melt inclusions, occasionally including microdiamonds and minor silicate phases, have been studied in diamond-bearing meta-carbonates from the Kokchetav Massif. They provide strong evidence that they represent trapped carbonate melts (Korsakov and Hermann, unpublished data).

7. Conclusions

The following conclusions can be drawn from the study of the C-polymorph micro-inclusions in garnet porphyroblasts from metapelites of the Rhodope Metamorphic Province by means of Raman microspectroscopy:

- The analytical proof of microdiamond inclusions in kyanite–biotite–garnet metapelites of the Greek Rhodope by means of in situ Raman micro-spectroscopy confirms that these rocks have undergone an ultrahigh-pressure metamorphism [1,6–8].
- The presence of diamond, cubic diamond–graphite composite inclusions, disordered graphite and highly ordered graphite in the same garnet porphyroblasts and the random distribution of graphite with different degree of graphitization exclude the possibility of prograde entrapment of increasingly ordered graphite during garnet growth and suggests that the *D* band in disordered graphite most probably arises from the distortion of the diamond structure during transformation to graphite. An octahedral or cubic habitus of graphite is the most convincing evidence for graphitized diamond. We interpret the transformation of diamond to graphite as continuous with the formation of disordered graphite as intermediate phase.
  Disordered graphite may have also precipitated from a combination of solid-state diamond–graphite transfor-

mation and reequilibration of primary fluid inclusions. Since crystallinity itself is insufficient to distinguish the origin of graphite further high resolution microscopy needs to be performed in order to clarify this issue.

- In the light of the present study, the controversial Raman spectrum presented by Mposkos and Kostopoulos [1] is likely that of disordered graphite formed after diamond.
  However, studying C-polymorphs with the 633 nm line of an He–Ne laser the possibility that a real diamond band is overlapped by graphite's *D* band in the rather intense band at 1332 cm^{-1} cannot be discounted.
- Of great interest is the presence of a C-phase, the Raman spectrum of which consists of a broad composite and asymmetric band at ~1330 cm^{-1} indicative of sp^3-hybridized C. The lack of a defined *G* band at ~1580 cm^{-1} differentiates this phase from graphitic carbon (sp^2-hybridized C), either amorphous or crystalline. High resolution TEM study would provide valuable and diagnostic information on the nanostructural characteristics of this C-phase (?nanodiamond, ?lonsdaleite, ? a different polymorph).
- Raman shift and FWHM of the F_{2g} phonon mode of metamorphic microdiamonds frequently deviate from the typical values for macroscopic diamonds which is attributed to variable particle size, internal stress variations, impurities and structural defects.
- Composite inclusions of diamond + carbonate, C-polymorph + CO_2 + carbonate, graphite + CO_2 and single diamond and graphite inclusions in swarm-like trails also containing carbonates and CO_2-rich fluids in garnet porphyroblasts imply that CO_2 and possibly C–O–H fluids were involved in the formation of diamond and disordered graphite.

Acknowledgements

We are thankful to C. Chopin and L. Nasdala for their critical comments and thorough and constructive review on the manuscript. We would like to thank D.C. Smith for valuable discussions. The financial support through the Austrian Science Fund (FWF-project P16194-No6) is highly acknowledged. Partial funding to MP provided by Hellenic State Scholarship Foundation (IKY) is gratefully appreciated. V. Courtillot is thanked for his editorial handling.

References

[1] E. Mposkos, D. Kostopoulos, Diamond, former coesite and supersilisic garnet in metasedimentary rocks from the Greek Rhodope: a new ultrahigh-pressure metamorphic province established, Earth Planet. Sci. Lett. 192 (2001) 497–506.
[2] N.J. Sobolev, V.S. Shatsky, Diamond inclusions in garnet from metamorphic rocks: a new environment for diamond formation, Nature 343 (1990) 742–746.
[3] L.F. Dobrzhinetskaya, E.A. Eide, R.B. Larsen, B.A. Sturt, R.G. Trønnes, D.C. Smith, W.R. Taylor, T.V. Posukhova, Microdiamond in high-grade metamorphic rocks of the Western Gneiss region, Norway, Geology 23 (1995) 597–600.
[4] L. Nasdala, H.J. Massonne, Microdiamonds from the Saxonian Erzgebirge, Germany: in situ micro-Raman characterisation, Eur. J. Mineral. 12 (2000) 495–498.
[5] J. Yang, Z. Xu, L. Dobrzhinetskaya, H.W. Green II, X. Pei, R. Shi, C. Wu, J.L. Wooden, J. Zhang, Y. Wan, H. Li, Discovery of metamorphic diamonds in central China: an indication of a >4000-km-long zone of deep subduction resulting from multiple continental collisions, Terra Nova 15 (2003) 370–379.
[6] E. Mposkos, D. Kostopoulos, M. Perraki, A. Proyer, R. Kaindl, G. Hoinkes, The Greek Rhodope: a new UHPM province, UHPM Workshop Waseda 3P10, 2001, pp. 218–222.
[7] E. Mposkos, Petrology of the ultra-high pressure metamorphic Kimi Complex in Rhodope (NE Greece): a new insight into the Alpine geodynamic evolution of the Rhodope, Bull. Geol. Soc. Greece 34 (2002) 2169–2188.
[8] A. Liati, D. Gebauer, R. Wysoczanski, U–Pb SHRIMP-dating of zircon domains from UHP garnet-rich mafic rocks and late pegmatoids in the Rhodope zone (N. Greece); evidence for Early Cretaceous crystallization and Late Cretaceous metamorphism, Chem. Geol. 184 (2002) 281–299.
[9] O. Beyssac, C. Chopin, Comment on "Diamond, former coesite and supersilisic garnet in metasedimentary rocks from the Greek Rhodope: a new ultrahigh-pressure metamorphic province established" by E.D. Mposkos and D.K. Kostopoulos, Earth Planet. Sci. Lett. 214 (2003) 669–674.
[10] C. Chopin, G. Ferraris, Mineral chemistry and mineral reactions in UHP, in: D.A. Carswell, R. Compagnoni (Eds.), Ultrahigh pressure metamorphism/EMU Notes Minerals, vol. 5, 2003, pp. 191–227.
[11] V. Jacobshagen, S. Durr, F. Kockel, K.O. Kopp, G. Kovalszyk, Structure and geodynamic evolution of the Aegean region, in: H. Closs, D. Roeder, K. Schmidt (Eds.), Alps Apennines, Hellenides IUCG Sci. Rept., vol. 38, 1978, pp. 537–564.
[12] F. Horvath, H. Beckhemer, Mediterranean back-arc basins, in: H. Beckhemer, K.J. Hsü (Eds.), Alpine Mediterranean Geodynamics, AGU Geodynamics Ser., vol. 7, 1982, pp. 141–173.
[13] B.C. Burchfiel, Eastern European Alpine system and the Carpathian orocline as an example of collision tectonics, Tectonophysics 63 (1980) 31–61.
[14] D. Papanikolaou, The three metamorphic belts of the Hellenides, in: J.E. Dixon, A.H.F. Robertson (Eds.), Geological Evolution of the Eastern Mediterranean, Geol. Soc. London, Spec. Publ., vol. 17, 1984, pp. 551–566.
[15] J.-P. Burg, L.E. Ricou, Z. Ivanov, I. Godfriaux, D. Dimov, L. Klain, Syn-metamorphic nappe complex in the Rhodope Massif. Structure and kinematics, Terra Nova 8 (1996) 6–15.
[16] L.E. Ricou, J.P. Burg, J. Godfriaux, Z. Ivanov, Rhodope and Vardar: the metamorphic and olistrostromic paired belts related to the Cretaceous subduction under Europe, Geodin. Acta 11 (1998) 285–309.
[17] E. Mposkos, High-pressure metamorphism in gneisses and pelitic schists in east Rhodope zone (N. Greece), Mineral. Petrol. 41 (1989) 337–351.

[18] E. Mposkos, A. Liati, Metamorphic evolution of metapelites in the high-pressure terrane of the Rhodope zone, Northern Greece, Can. Mineral. 31 (1993) 401–424.
[19] E. Mposkos, N. Wawrzenitz, Metapegmatites and pegmatites bracketing the time of HP-metamorphism in polymetamorphic rocks of the E-Rhodope, N. Greece: petrological and geochronological constraints, Spec. Publ. - Geol. Soc. Greece 24 (1995) 602–608.
[20] D. Gebauer, A. Liati, Geochronological evidence for Mesozoic rifting and oceanization followed by Eocene subduction in the Rhodope Complex (northern Greece), Terra Nova 9 (Abstract supplement No.1) (1997) 10.
[21] N. Wawrzenitz, A. Krohe, Exhumation and doming of the Thasos Metamorphic Core Complex (S. Rhodope, Greece): structural and geochronological constraints, Tectonophysics 285 (1998) 301–332.
[22] D.A. Dinter, Late Cenozoic extension of the Alpine collisional orogen, northeastern Greece: origin of the north Aegean basin, Geol. Soc. Amer. Bull. 110 (1998) 1208–1230.
[23] S.R. Barr, S. Temperley, J. Tarney, Lateral growth of the continental crust through deep level subduction–accretion: a re-evaluation of central Rhodope, Lithos 46 (1999) 69–94.
[24] A. Liati, D. Gebauer, Constraining the prograde and retrograde *P–T–t* path of Eocene HP-rocks by SHRIMP dating of different zircon domains: inferred rates of heating, burial, cooling and exhumation for central Rhodope, northern Greece, Contrib. Mineral. Petrol. 135 (1999) 340–354.
[25] E. Mposkos, A. Krohe, Petrological and structural evolution of continental high pressure (HP) metamorphic rocks in the Alpine Rhodope Domain (N. Greece), in: I. Panayides, C. Xenophontos, J. Malpas (Eds.), Proc. 3rd Int. Conf. Geol. E. Mediterranean, Nicosia, Cyprus, 2000, pp. 221–232.
[26] A. Krohe, E. Mposkos, Multiple generations of extensional detachments in the Rhodope Mountains (N. Greece): evidence of episodic exhumation of high-*P* rocks, in: D.J. Blundell, G. Neubauer, A. Von Quant (Eds.), The Timing and Location of Major Ore Deposits in an Evolving Orogen, Geological Society of London, Special Publication, vol. 204, 2002, pp. 151–178.
[27] E. Mposkos, Interpretation of metamorphic paths of the lower and upper tectonic unit of Rhodope: similarities and differences, Bull. Geol. Soc. Greece 31/1 (1994) 255–269 (In Greek with English abstract).
[28] R. Kaindl, M. Perraki, A. Proyer, G. Hoinkes, CO_2-inclusions in metapelitic garnets of the ultrahigh-pressure Rhodope metamorphic province, NE Greece, 32nd Int. Geol. Congr., 2004, p. 414, Abs. Vol., pt.1, abs. 84-3.
[29] M. Perraki, A. Proyer, E. Mposkos, R. Kaindl, I. Baziotis, G. Hoinkes, Micro- and nanodiamonds in garnets of metapelitic rocks from the Greek Rhodope: an in situ micro-Raman study, in: A.A. Chatzipetros, S.S. Pavlides (Eds.), Proceedings of the 5th International Symposium on Eastern Mediterranean Geology, 2004, pp. 1216–1219.
[30] L. Nasdala, W. Hofmeister, J.W. Harris, J. Glinnemann, Growth zoning and strain patterns inside diamond crystals as revealed by Raman maps, Am. Mineral. 90 (2005) 745–748.
[31] P. Knoll, R. Singer, W. Kiefer, Improving spectroscopic techniques by a scanning multichannel method, Appl. Spectrosc. 44 (1990) 776–782.
[32] G. Irmer, Zum Einfluss der Apparatefunktion auf die Bestimmung von Streuquerschnitten und Lebensdauern aus optischen Phononenspektren, Exp. Tech. Phys. 33 (1985) 501–506.
[33] P. Verma, S.C. Abbi, K.P. Jain, Raman-scattering probe of anharmonic effects in GaAs, Phys. Rev., B 51 (1995) 16660–16667.
[34] L. Nasdala, M. Wenzel, G. Vavra, G. Irmer, T. Wenzel, B. Kober, Metamictization of natural zircon: accumulation versus thermal annealing of radioactivity-induced damage, Contrib. Mineral. Petrol. 141 (2001) 125–144.
[35] S.A. Solin, A.K. Ramdas, Raman spectrum of diamond, Phys. Rev., B 1 (1970) 1687–1698.
[36] L.C. Prinsloo, Infrared and Raman spectroscopy, in: S. Kalbitzer (Ed.), Diamond for High-Density Optical Recording, Appl. Phys. A, 2001, pp. 639–670.
[37] Ph. Gillet, R.I. Hemley, P.F. McMillan, Vibrational properties at high pressures and temperatures, in: R.I. Hemley (Ed.), Ultrahigh-Pressure Mineralogy, Mineralogical Society of America, Washington DC, 1998, pp. 525–581.
[38] F. Tuinstra, J.L. Koenig, Raman spectrum of graphite, J. Chem. Phys. 53 (1970) 1126–1130.
[39] R.J. Nemanich, S.A. Solin, First- and second-order Raman scattering from finite-size crystals of graphite, Phys. Rev., B 20 (1979) 392–401.
[40] A.C. Ferrari, J. Robertson, Interpretation of Raman spectra of disordered and amorphous carbon, Phys. Rev., B 61 (2000) 14095–14107.
[41] P. Lespade, R. Al-Jishi, M.S. Dresselhaus, Model for Raman scattering from incompletely graphitized carbons, Carbon 5 (1982) 427–431.
[42] Y. Wang, D.C. Alsmeyer, R.L. McCreery, Raman spectroscopy of carbon materials: structural basis of observed spectra, Chem. Mater. 2 (1990) 557–563.
[43] J.D. Pasteris, B. Wopenka, Raman spectra of graphite as indicators of degree of metamorphism, Can. Mineral. 29 (1991) 1–9.
[44] B. Wopenka, J.D. Pasteris, Structural characterization of kerogens to granulite-facies graphite: applicability of Raman microprobe spectroscopy, Am. Mineral. 78 (1993) 533–577.
[45] C. Beny-Bassez, J.N. Rouzaud, Characterization of Carbonaceous Materials by Correlated Electron and Optical Microscopy and Raman Micro-Spectroscopy, Scanning Electron Microscopy, SEM Inc., Chicago, 1985, pp. 119–132.
[46] R.P. Vidano, D.B. Fischbach, L.I. Willis, T.M. Loehr, Observation of Raman band shifting with excitation wavelength for carbons and graphites, Solid State Commun. 39 (1981) 341–344.
[47] Y. Kawashima, G. Katagiri, Fundamentals, overtones, and combinations in the Raman spectrum of graphite, Phys. Rev., B 52 (1995) 10053–10059.
[48] M.J. Matthews, M.A. Piments, G. Dresselhaus, M.S. Dresselhaus, M. Endo, Origin of dispersive effects of the Raman *D* band in carbon materials, Phys. Rev., B 59 (1999) 6585–6588.
[49] C. Thomsen, S. Reich, Double resonant Raman scattering in graphite, Phys. Rev. Lett. 85 (24) (2000) 5214–5217.
[50] Ph. Gillet, C. Bielmann, B. Reynard, P.F. McMillan, Raman spectroscopic studies of carbonates. Part I: high-pressure and high-temperature behaviour of calcite, magnesite, dolomite, aragonite, Phys. Chem. Miner. 20 (1993) 1–18.
[51] O. Beyssac, B. Goffe, C. Chopin, J.N. Rouzaud, Raman spectra of carbonaceous material in metasediments: a new geothermometer, J. Metamorph. Geol. 20 (2002) 859–871.
[52] H.N Rutt, J.H. Nicola, Raman spectra of carbonates of calcite structure, J. Phys. C. Solid State Phys. 7 (1974) 4522–4528.

[53] E.A.J. Burke, Raman micro-spectroscopy of fluid inclusions, Lithos 55 (2001) 139–158.
[54] Y. Garrabos, R. Tufev, B. Le Neindre, G. Zalczer, D. Beysens, Rayleigh and Raman scattering near the critical point of carbon dioxide, J. Chem. Phys. 72 (1980) 4637–4651.
[55] A.M. van den Kerkhof, S.N. Olsen, A natural example of superdense CO_2 inclusions: microthermometry and Raman analysis, Geochim. Cosmochim. Acta 54 (1990) 895–901.
[56] M.L. Frezzotti, E.A.J. Burke, B. De Vivo, B. Stefanini, I.M. Villa, Mantle fluids in pyroxenite nodules from Salt Lake Crater, Oahu, Hawaii, Eur. J. Mineral. 4 (1992) 1137–1153.
[57] H. Schneiderhoehn, Erzmikroskopisches Praktikum, Schweizerbart'sche Verlagsbuchhandlung, Stuttgart, 1952, 274 pp.
[58] J.D. Pasteris, In situ analysis in geological thin-sections by laser Raman microprobe micro-spectroscopy: a cautionary note, Appl. Spectrosc. 43 (1989) 567–570.
[59] T.F. Yui, E. Huang, J. Xu, Raman spectrum of carbonaceous material: a possible metamorphic grade indicator for low-grade metamorphic rocks, J. Metamorph. Geol. 14 (1996) 115–124.
[60] O. Beyssac, J.N. Rouzaud, B. Goffe, F. Brunet, C. Chopin, Graphitization in a high-pressure, low-temperature metamorphic gradient: a Raman micro-spectroscopy and HRTEM study, Contrib. Mineral. Petrol. 143 (2002) 19–31.
[61] F.J. Luque, J.D. Pasteris, B. Wopenka, M. Rodas, J.F. Barrenechea, Natural fluid-deposited graphite: mineralogical characteristics and mechanisms of formation, Am. J. Sci. 298 (1998) 471–498.
[62] A. Wang, P. Dhamelincourt, J. Dubessy, D. Guerard, P. Landais, M. Lelaurain, Characterization of graphite alteration in an uranium deposit by micro-Raman spectroscopy, X-ray diffraction, transmission electron microprobe and scanning electron microscopy, Carbon 27 (1989) 209–218.
[63] L. Nasdala, D.C. Smith, R. Kaindl, M.A. Ziemann, Raman spectroscopy: analytical perspectives in mineralogical research, in: A. Beran, E. Libowitzky (Eds.), EMU Notes in Mineralogy, Spectroscopic Methods in Mineralogy, vol. 6, 2004, pp. 281–344.
[64] J.D. Pasteris, I.M. Chou, Fluid-deposited graphitic inclusions in quartz: comparison between KTB (German Continental Deep-Drilling) core samples and artificially reequilibrated natural inclusions, Geochim. Cosmochim. Acta 62 (1998) 109–122.
[65] Y.G. Gogotsi, A. Kailer, K.G. Nickel, Pressure-induced phase transformation in diamond, J. Appl. Phys. 84 (1998) 1299–1304.
[66] Y.G. Gogotsi, A. Kailer, K.G. Nickel, Transformation of diamond to graphite, Nature 401 (1999) 663–664.
[67] T. Kenkmann, U. Hornemann, D. Stoeffler, Transformation of graphite to diamond in shock experiments: a Raman study, Lunar Planet. Sci. XXXIII (2002) 1052.
[68] A. El Goresy, P. Gillet, M. Chen, F. Kuenstler, G. Graup, V. Staehle, In situ discovery of shock-induced graphite-diamond phase transition in gneisses from the Ries Crater, Germany, Am. Mineral. 86 (2001) 611–621.
[69] M.L. Leech, W.G. Ernst, Graphite pseudomorphs after diamond? A carbon isotope and spectroscopic study of graphite cuboids from the Maksyutov Complex, south Ural Mountains, Russia, Geochim. Cosmochim. Acta 62 (1998) 2143–2154.
[70] B. Willems, K. De Corte, G. Van Tendeloo, Why does polycrystalline natural diamond turn black after annealing?, Phys. Status Solidi, A Appl. Res. 201 (2004) 2486–2491.
[71] J. Fayos, Possible 3D carbon structures as progressive intermediates in graphite to diamond phase transition, J. Solid State Chem. 148 (1999) 278–285.
[72] C.P. Ewels, N.T. Wilson, M.I. Heggie, R. Jones, P.R. Briddon, Graphitization of diamond dislocation cores, J. Phys., Condens. Matter 13 (2001) 8965–8972.
[73] M. Satish-Kumar, Graphite-bearing CO_2-fluid inclusions in granulites: insights on graphite precipitation and carbon isotope evolution, Geochim. Cosmochim. Acta 69 (2005) 3841–3856.
[74] M. Yoshikawa, Y. Mori, H. Obata, M. Maegawa, G. Katagiri, H. Ishida, A. Ishitani, Raman scattering from nanometer-sized diamond, Appl. Phys. Lett. 67 (1995) 694–696.
[75] J. Chen, S.Z. Deng, L. Chen, Z.X. Yu, N.S. Xu, Graphitization of nanodiamond powder annealed in argon ambient, Appl. Phys. Lett. 74 (1999) 3651–3653.
[76] S. Prawer, K.W. Nugent, D.N. Jamieson, J.O. Orwa, L.A. Bursill, J.L. Peng, The Raman spectrum of nanocrystalline diamond, Chem. Phys. Lett. 332 (2000) 93–97.
[77] T.N. Moroz, E.N. Fedorova, S.M. Zhmodik, A.G. Mironov, G.M. Rylov, A.L. Ragozin, A.D. Afanasyev, V.J. Zaikovsky, Investigation of various carbon modifications by means of Raman spectroscopy, Chem. Sustain. Dev. 8 (2000) 43–47.
[78] B.C. Bostick, R.E. Jones, W.G. Ernst, C. Chen, M.L. Leech, R.J. Beane, Low-temperature microdiamond aggregates in the Maksyutov Metamorphic Complex, South Ural Mountains, Russia, Am. Mineral. 88 (2003) 1709–1717.
[79] C.V. Chiem, H.-K. Seo, S.G. Ansari, G.-S. Kim, J.M. Seo, H.-S. Shin, Lonsdaleite diamond growth on reconstructed Si (100) by hot-filament chemical vapour deposition (HFCVD), Korean J. Chem. Eng. 20 (2003) 1154–1157.
[80] D.C. Smith, Raman mapping of chemical and/or physical mineral phase transformations involving jadeite, coesite, diamond or zircon in natural ultra-high pressure metamorphic environments (UHPM), in: P.M. Fredericks, R.L. Frost, L. Rintoul (Eds.), Plenary lecture, XIXth International Conference on Raman Spectroscopy, ICORS, Gold Coast, Australia, 8-13, Proceedings, August 2004, CD-ROM.
[81] G. Godard, D. Smith, M. Moreau, Raman mapping of microdiamond and other carbon phases included in zircons in a Norwegian eclogite, 32nd Int. Geol. Congr., 2004, p. 720, Abs. Vol., pt.1, abs. 153-2.
[82] D.S. Knight, W.B. White, Characterization of diamond films by Raman spectroscopy, J. Mater. Res. 4 (1989) 385.
[83] H. He, T. Sekine, T. Kobayashi, Direct transformation of cubic diamond to hexagonal diamond, Appl. Phys. Lett. 81 (2002) 610–612.
[84] C. Frondel, U.B. Marvin, Lonsdaleite, a new hexagonal polymorph of diamond, Nature 214 (1967) 587–589.
[85] P. Badziag, W.S. Verwoerd, W.P. Ellis, N.R. Griener, Nanometre-sized diamonds are more stable than graphite, Nature 343 (1990) 244.
[86] H. Ishida, Y. Ogasawara, K. Ohsumi, A. Saito, Two stage growth of microdiamond in UHP dolomite marble from Kokchetav Massif, Kazakhstan, J. Metamorph. Geol. 21 (2003) 515–522.
[87] A.V. Korsakov, P. Vandenabeele, K. Theunissen, Discrimination of metamorphic diamond populations by Raman spectroscopy (Kokchetav, Kazakhstan), Spectrochim. Acta A 61 (2005) 2378–2385.
[88] N.V. Surovtsev, I.N. Malinovsky, V.A. Gusev, Yu.N. Pal'yanov, Effect of nitrogen impurities on the Raman line width in diamonds, J. Phys., Condens. Matter 11 (1999) 4767–4774.

[89] X.Z. Zhao, K.A. Cherian, R. Roy, W.B. White, Downshift of Raman peak in diamond powders, J. Mater. Res. 13 (1998) 1974–1976.
[90] M. Akaishi, M.D. Shaji Kumar, H. Kanda, S. Yamaoka, Formation process of diamond from supercritical H_2O–CO_2 fluid under high pressure and high temperature conditions, Diamond Relat. Mater. 9 (2000) 1945–1950.
[91] S. Yamaoka, M.D. Shaji Kumar, H. Kanda, M. Akaishi, Formation of diamond from $CaCO_3$ in a reduced C–O–H fluid at HP–HT, Diamond Relat. Mater. 11 (2002) 1496–1504.
[92] K. De Corte, A. Korsakov, W.R. Taylor, P. Cartigny, M. Ader, P. De Paepe, Diamond growth during ultrahigh-pressure metamorphism of the Kokchetav Massif, northern Kazakhstan, Isl. Arc 9 (2000) 428–438.
[93] B. Stoeckhert, J. Duyster, C. Trepmann, H.-J. Massonne, Microdiamond daughter crystals precipitated from supercritical COH-silicate fluids included in garnet, Erzgebirge, Germany, Geology 29 (2001) 391–394.
[94] L.F. Dobrzhinetskaya, H.W. Green, K.N. Bozhilov, T.E. Mitchell, R.M. Dickerson, Crystallization environment of Kazakhstan microdiamond: evidence from nanometric inclusions and mineral associations, J. Metamorph. Geol. 21 (2003) 425–437.
[95] M. Akaishi, H. Kanda, S. Yamaoka, Synthesis of diamond from graphite–carbonate system under very high temperature and pressure, J. Cryst. Growth 104 (1990) 578–581.
[96] K. Sato, M. Akaishi, S. Yamaoka, Spontaneous nucleation of diamond in the system $MgCO_3$–$CaCO_3$–C at 7.7 GPa, Diamond Relat. Mater. 8 (1999) 1900–1905.
[97] Y. Pal'yanov, A. Sokol, Y. Borzdov, A. Khokhryakov, N. Sobolev, Diamond formation from mantle carbonate fluids, Nature 400 (1999) 417–418.
[98] Y. Pal'yanov, A. Sokol, Y. Borzdov, A. Khokhryakov, N. Sobolev, Diamond formation through carbonate–silicate interaction, Am. Mineral. 87 (2002) 1009–1013.
[99] J. Siebert, F. Guyot, V. Malavergne, Diamond formation in metal-carbonate interactions, Earth Planet. Sci. Lett. 229 (2005) 205–216.
[100] Y. Ogasawara, M. Ohta, H. Ishida, K. Fukasawa, Unique high pressure evidence in the Kokchetav UHP carbonate rocks, in: Abstract of Goldschmidt Conference, vol. 3545, 2001.